communications biology

A Nature Portfolio journal

Article

https://doi.org/10.1038/s42003-025-08324-0

Forward and convergent remapping of receptive fields from local field potentials in frontal eye fields

Min Jin[1], Lin Yang[1], Fangfang Jia[1], Ning Qian[2] & Mingsha Zhang[1]

Receptive-field (RF) remapping, produced by attention and corollary discharges (CDs) of saccade commands, has been found in many brain areas. Most remapping studies use neurons' firing rates of spikes to determine their RFs, and relatively less is known about the remapping behavior of RFs derived from local field potentials (LFPs) which include contributions of synaptic inputs. Here we use LFPs to measure RF remapping in frontal eye fields (FEF) of macaques while they perform a delayed saccade task. We focus on the high-gamma and alpha bands of the LFPs because RFs from these bands show reliable remapping. We find that during the delay period, the high-gamma RFs shift towards the initial fixation point. During the perisaccadic period, the high-gamma RFs first shift towards the target (convergent remapping), then towards the post-saccadic RF locations (forward remapping), and finally towards the target again. These results are consistent with those of the firing-rate-defined RFs, with presumably attention-driven convergent remapping and CD-driven forward remapping occurring at different times. In contrast, the alpha RFs show no significant remapping in the delay period and only forward remapping throughout the perisaccadic period. To the extent that the high-gamma and alpha bands of LFPs may reflect synaptic inputs from local circuits and other brain areas, respectively, these results suggest that attentional remapping may be generated locally in FEF whereas forward remapping may have both local and distant contributions.

It has long been recognized that receptive fields (RFs) are not static but can undergo dynamic changes. An example is perisaccadic RF remapping found in many brain areas including frontal eye fields (FEF)[1–5], lateral intraparietal cortex (LIP)[4–7], middle temporal area (MT)[8,9], V4[8,10,11], V3[12], V2[13], and superior colliculus (SC)[14,15]. Early remapping studies found that some cells show visual responses at their future (post-saccadic) RF (fRF) locations, accompanied by reduced responses at the current (pre-saccadic) RF (cRF) locations, even before the saccadic onset. Later studies examined the remapping time course[4,5,7,11]. It was found that in LIP and FEF, cells' perisaccadic RFs (pRFs) shift progressively from their cRF locations to their fRF locations over time (from 50–100 ms before the saccade to 50–100 ms after the saccade). Since stimuli for measuring pRFs are flashed before the saccadic onset, the pRF remapping time course cannot have contributions from reafferent retinal inputs after the saccadic onset and must be driven by corollary discharge (CD) of saccade commands[4,6,7]. Sommer and Wurtz provided evidence that perisaccadic remapping in FEF indeed depends on CDs from SC via thalamus[1].

In addition to the CD-driven remapping, RFs also shift towards attentional loci[4,11,16–18], sometimes termed convergent[19] or compressive remapping. Zirnsak et al. argued that perisaccadic remapping in FEF is all convergent shift towards the saccade target, without the forward shift towards the fRF discussed above[18]. Using a delayed saccade task to separate the target onset and the saccade initiation, we recently found that in LIP and FEF, both convergent and forward RF shifts occur but at different times[4]: During the delay period, the remapping direction appears to follow attention from the initial fixation point to the saccade target. During the perisaccadic period, the remapping direction was towards the target shortly after the stimulus onset but becomes predominantly towards the fRF around the saccadic onset/offset when the CD is presumably present. Through computational modeling, we showed that the convergent and forward remapping can be explained by attention-modulated center-excitation/surround-inhibition connections and CD-gated directional connections, respectively, and that both sets of connections emerge automatically in recurrent neural networks trained to update retinal positions of stimuli across saccades, a task related to transsaccadic visual stability.

[1]Key Laboratory of Cognitive Neuroscience and Learning, Division of Psychology, Beijing Normal University, Beijing, China. [2]Department of Neuroscience and Zuckerman Institute, Columbia University, New York, NY, USA. e-mail: mingsha.zhang@bnu.edu.cn

Most studies of RF remapping used firing rates of neurons' spiking activities to define RFs. Relatively few studies examined the remapping of RFs derived from local field potentials (LFPs). Exceptions include the works of Chen et al. and Neupane et al.[11,20,21]. In contrast to spiking activities of single neurons, LFPs may reflect synaptic activities of the neuronal population within hundreds of millimeters around the electrode[22–24]. Additionally, high and low frequency bands of LFPs may reflect synaptic inputs from local circuits and other brain areas, respectively[25,26]. It may thus be interesting to examine remapping of RFs defined by LFPs. To our knowledge, only one study explored the remapping of LFP-defined RFs in FEF[20]. The authors reported that the pRFs derived from both the alpha and high-gamma bands of LFPs converge towards the saccade target only, consistent with the remapping of the firing-rate-defined RFs reported by the same lab[18], and that the convergence of the alpha pRFs is later than that of the high-gamma and firing-rate pRFs. However, as we noted above, by using a delayed saccade task and examining the detailed remapping time course, we found both convergent and forward remapping in the firing-rate-defined RFs in FEF[4].

In this study, we therefore investigated whether the LFP-defined RFs in FEF also showed both types of remapping in a delayed saccade task. We found that alpha RFs shifted consistently towards fRF (forward remapping), whereas high-gamma RFs showed temporally dynamic remapping, progressing from the initial fixation point to the saccade target (convergent remapping), then to the fRF, and back to the saccade target. These results suggested that attentional remapping (convergent remapping) might be generated locally in FEF, whereas forward remapping might have both local and distant contributions.

Results

RFs simultaneously measured with firing rates and the alpha and high-gamma bands of LFPs overlapped with each other

We measured the RFs derived from the following four frequency bands of the LFPs: alpha (8–12 Hz), beta (12–30 Hz), low-gamma (30–80 Hz) and high-gamma band (80–150 Hz) in a delayed saccade task (Fig. 1b). Over 430 recording sessions in FEF, 33.0% of alpha band RFs, 32.8% of beta band RFs, 16.0% of low-gamma band RFs, and 43.0% of high-gamma band RFs were well defined (see "Methods") during the current period. We compared the spatial profiles of the RFs defined by the firing rates and LFPs recorded from the same sessions. An example is shown in Fig. 2a. The first panel shows the firing-rate-defined RF, and the second to the fifth panels show the RFs derived from the alpha, beta, low-gamma, and high-gamma bands of the LFPs, respectively. In each panel, the heat map represents responses across probe locations and the cyan and black crosses denote the fixation point and the RF center, respectively. For this recording, the RFs derived from the firing rates and different bands of the LFPs largely overlapped with each other.

To quantify similarities among these RFs, for each recording site, we calculated the Pearson correlation coefficient between the firing-rate RF and each of the four RFs derived from the four frequency bands of the LFPs. The distributions of the correlation coefficients are shown in the four columns of Fig. 2b. Across the recording sessions, the mean correlations were significantly different from 0 for the alpha, beta, low-gamma and the high-gamma bands ($\bar{r}_{\text{alpha, spikes}} = 0.46, p < 10^{-21}$; $\bar{r}_{\text{beta, spikes}} = 0.35, p < 10^{-21}$; $\bar{r}_{\text{low-gamma, spikes}} = 0.20, p < 10^{-8}$; $\bar{r}_{\text{high-gamma, spikes}} = 0.55, p < 10^{-31}$, Wilcoxon signed rank test). We also employed the permutation test to determine whether each individual pair of the RFs above was significantly correlated (see "Methods"). The significant and non-significant counts are indicated by the blue and orange colors, respectively, in Fig. 2b. The proportions of the recording sessions with significant correlations between the firing-rate RFs and the alpha RFs, beta RFs, low-gamma RFs, and high-gamma RFs were, respectively, 72.5% (103/142), 63.1% (89/141), 31.9% (22/69), and 87.0% (161/185). Thus, among the four frequency bands, the RFs derived from the alpha and high-gamma bands were in better agreement with the corresponding RFs derived from the firing rates. These results are consistent with previous findings[20].

Remapping of alpha and high-gamma RFs during the delay and perisaccadic periods

We define the forward direction as the direction from the cRF center to the corresponding fRF center, and the remapping as the shifts of the dRF or pRF center relative to the cRF center[4]. To investigate the remapping of RFs derived from LFPs, we need well-defined RFs during the current, delay, perisaccadic, and future periods, and a significant shift of the dRF or pRF center relative to the corresponding cRF center. Table 1 shows the number

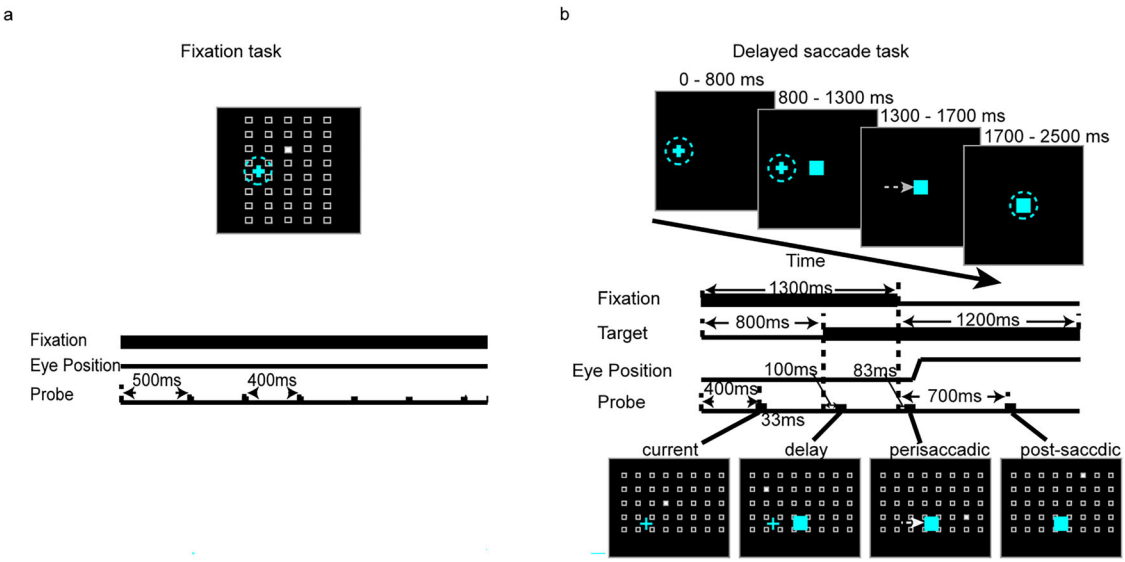

Fig. 1 | Behavioral tasks. The cyan cross, cyan square, cyan dashed circle, and gray arrow represent the initial fixation point, saccade target, eye position, and saccade vector, respectively. **a** Fixation task. Top panel: the screen with the fixation point. Middle panel: the time interval between the acquisition of the fixation point and the appearance of the first probe is 500 ms and that between two successive probes is 400 ms. Bottom panel: the open squares denote the array of all possible probe locations, whereas the white square denotes the location of an example probe. **b** Delayed saccade task. Top panel: the trial sequence. Middle panel: the detailed time course. In each trial, four probes were flashed, one for each of the four periods: current, delay, perisaccadic, and future (post-saccadic). The RFs measured from these periods are named as cRF, dRF, pRF, and fRF, respectively; Bottom panel: the format is the same as that in (**a**).

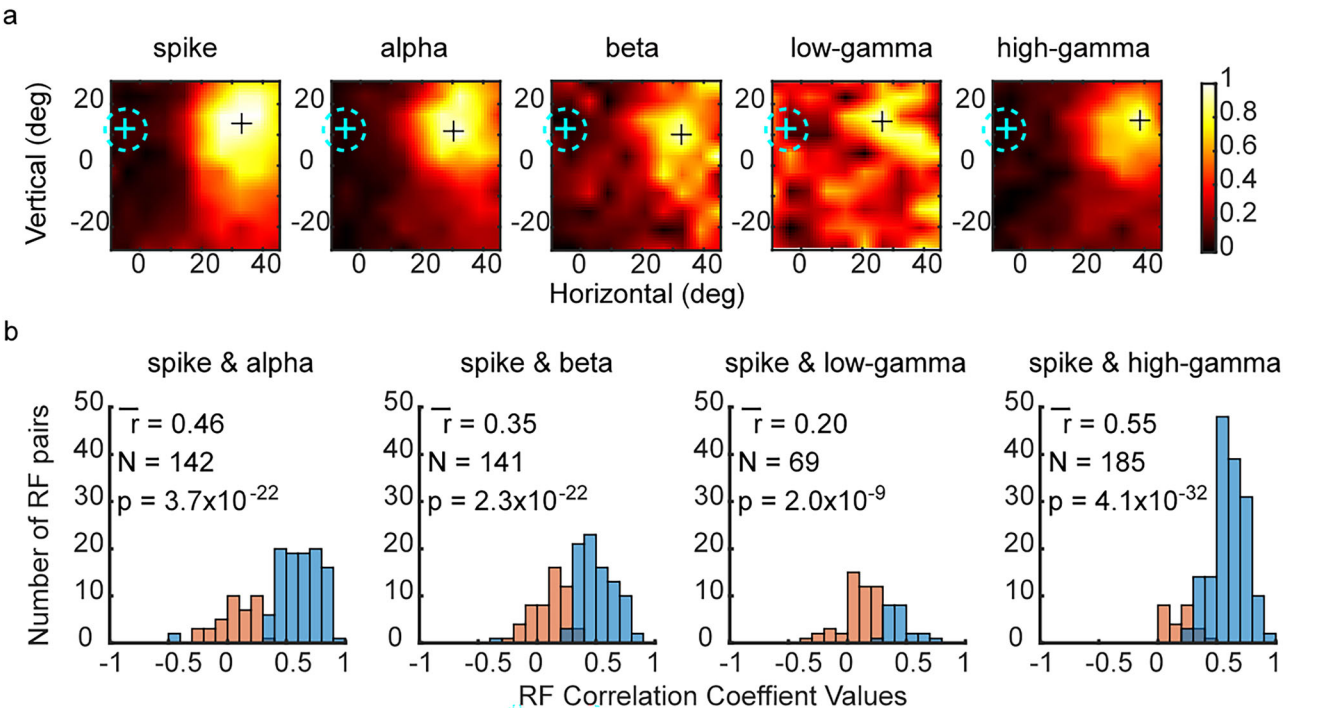

Fig. 2 | The comparison between the firing-rate RFs and the alpha, beta, low-gamma, and high-gamma RFs from the same recording sessions during the current period. The cyan and black cross represent the fixation point and the RF center, respectively. The cyan dashed circle represents the required eye position. **a** An example of the firing-rate, alpha, beta, low-gamma, high-gamma RFs from the same recording site. **b** Distributions of the correlation coefficients between the firing-rate RF and each of the RFs derived from the alpha, beta, low-gamma, and high-gamma frequency bands of the LFPs in FEF. *N*: the number of total recording sessions with well-defined RFs during the current period. Blue and orange colors indicate counts of significant and non-significant correlation between a pair of RFs according to the permutation test.

Table 1 | The number of recording sessions with significant RF remapping during the delay and perisaccadic periods

	dRF probe on 0 to 250 ms	pRF1 probe on 0 to 250 ms	pRF2 sac. off −125 to 125 ms	pRF3 sac. off 0 to 250 ms	pRF4 sac. off 125 to 375 ms
Alpha	46	48	47	43	37
Beta	22	26	26	21	17
Low-gamma	4	3	6	4	4
High-gamma	34	33	31	37	31

of recording sessions in which a dRF or pRF showed significant remapping in various time windows of the delay or perisaccadic periods. As detailed in the "Methods" section, for each session and frequency band, we used bootstrapping to calculate the distributions of the RF centers and determined whether or not a remapping vector is significant. Since there were more sessions with significant remapping for the RFs derived from the alpha and high-gamma bands but very few sessions with remapping in beta and low-gamma bands, we focused on RFs derived from alpha and high-gamma bands for the rest of the analysis.

The alpha and high-gamma RFs from two different recording sessions are shown in Fig. 3a, b, respectively. The figure format is the same as that of Fig. 2a, with an additional cyan dashed line and arrow line in each panel representing the shift of RF's centers and saccadic direction, respectively. The alpha and high-gamma RFs exhibited different remapping behaviors. During the delay period, the alpha dRF's center at ($x = 6.9$, $y = 3.1$) did not show a clear shift (Fig. 3a, second column) relative to its cRF center at ($x = 9.0$, $y = 2.7$), whereas the high-gamma dRF's center at ($x = 27.0$, $y = 15.0$) shifted clearly towards the initial fixation point at ($x = -5$, $y = 12$) (Fig. 3b, second column) relative to its cRF center at ($x = 38.6$, $y = 14.8$). Throughout the perisaccadic period (Fig. 3a, third to sixth columns; the time periods for pRF1 to pRF4 are defined in Table 1), the alpha pRFs exhibited forward shift towards the fRF's center at ($x = 8.8$, $y = 15.0$), with the pRF1's center at ($x = 8.6$, $y = 8.3$), pRF2's center at ($x = 8.7$, $y = 9.5$), pRF3's center at ($x = 8.8$, $y = 10.1$) and pRF4's center at ($x = 9.0$, $y = 9.5$). However, the remapping direction of the high-gamma pRFs changed over time, i.e., gradually from towards saccade target to fRF (Fig. 3b, from third to sixth column). In more detail, the pRF1's center at ($x = 33.0$, $y = 9.0$) shifted towards the saccade target at ($x = -5$, $y = -18$), the pRF2's center at ($x = 26.5$, $y = -9$) shifted towards the direction between saccade target and fRF at (35.3, −13.2), the pRF3's center at ($x = 31.3$, $y = -10.0$) shifted primarily towards the direction of fRF, and finally, the pRF4's center at ($x = 21.3$, $y = -21.3$) shifted in a direction between the saccade target and fRF.

To illustrate the population results, we present the directions of RF remapping as polar plots in Fig. 4a. In each polar plot, we aligned the cRFs of recording sessions at the center and saccade directions along the positive horizontal. The mean fRF (forward), target (convergent), and initial-fixation directions are indicated by the blue, red, and green squares, respectively. Each dot represents the RF shift direction of a recording session, and the thick black line represents the circular mean whose significance was indicated by the *p* values from Rayleigh test. The dashed gray lines mark the 95% confidence interval of the mean direction. The circular histogram shows the distribution of the shift directions of the recording sessions. The corresponding shift vectors are shown in Fig. 4b. The fRF center, the saccade target and fixation point of a recording session are shown as blue, red and green dots, respectively. Their mean positions are indicated by the blue, red,

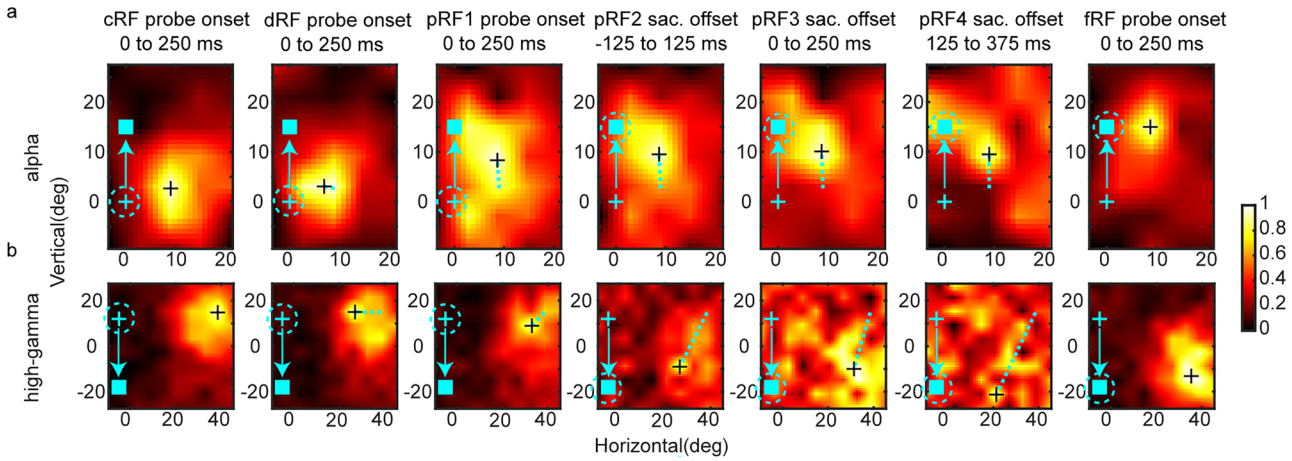

Fig. 3 | Example RFs derived from alpha and high-gamma band during different periods in FEF. a Example RFs derived from alpha band. **b** Example RFs derived from high-gamma band. The cyan cross and square indicate the fixation point and saccade target, respectively. The cyan dotted circle indicates the eye position. The small black cross marks the RF center. The cyan dashed lines and arrows in heatmaps from different periods indicate the shift of RF center related to cRF and saccade direction, respectively. The scale of normalized responses is shown on the right. The pRF1, pRF2, pRF3 and pRF4 during perisaccadic period were estimated from 0 to 250 ms after perisaccadic probe onset, and from −125 to 125 ms, 0 to 250 ms and 125 to 375 ms relative to the saccadic offset, respectively.

and green squares, respectively. Each gray arrow represents the RF shift vector for each recording session.

The alpha and high-gamma RFs remapped differently at the population level (Fig. 4). For the alpha band (the first row of Fig. 4a), there was no significant remapping in dRF and pRF1 (p values of Rayleigh test in each panel), so we focused on the mean RF remapping directions during the later perisaccadic periods. The mean remapping directions of pRF2, pRF3 and pRF4 were primarily towards the mean direction of the fRFs, and were not significantly different from the mean directions of fRFs but significantly different from saccade targets except pRF2 (one-sample test, Circular Statistics Toolbox in Matlab). In addition, we applied a Watson-Williams multi-sample test to examine whether there were significant changes in the remapping direction across perisaccadic periods. We chose pRF2 and pRF4 for this test because they showed significant remapping and we excluded pRF3 to avoid temporal overlaps (Table 1). The results showed that there were no significant changes in mean RF remapping directions ($p = 0.54$, $F_{(1, 82)} = 0.37$).

For the high-gamma band (the second row of Fig. 4a), the mean remapping direction of dRFs was significantly different from the mean directions of fRF and saccade target, but was not significantly different from the direction of initial fixation point (one-sample test, Circular Statistics Toolbox for Matlab). Although the mean pRF1 remapping direction was not significantly different from either the mean directions of the fRFs or the saccade target, it was close to the direction of saccade target. The mean remapping directions of pRF2 and pRF3 were not significantly different from the mean directions of fRFs, but were significantly different from saccade targets. Finally, the mean remapping direction of pRF4 was significantly different from the mean direction of fRF, but not from saccade target. Additionally, we examined whether the mean remapping directions changed significantly during delay and perisaccadic intervals by using Watson-Williams multi-sample test. We chose dRF, pRF2 and pRF4 for this test because they showed significant remapping and we excluded pRF1 and pRF3 to avoid temporal overlaps. The results showed significant changes in remapping direction across these periods ($p = 3.0 \times 10^{-11}$, $F_{(2, 93)} = 31.8$).

To demonstrate the robustness of our results, we varied the key parameters that determine the contour and completeness of RFs and the remapping of the RFs (see "Method" for details) and repeated the same analysis as we did for Fig. 4. The results (Supplementary Figs. 2–4) were generally consistent with those in Fig. 4.

Since the forward and convergent remapping are, by definition, toward the fRF and the target, respectively, we determined whether a pRF center is closer to the fRF center or the target. The results are shown in Fig. 5. For the alpha band and four pRF periods, the pRF-to-fRF distance was significantly shorter than the pRF-to-target distance (see the p values in Fig. 5), suggesting that the forward remapping is stronger than the convergent remapping during the perisaccadic period. For the high-gamma band, the difference was significant for the pRF3 period but not the other periods, consistent with the changing remapping direction of this band shown in Fig. 4.

Finally, we analyzed the remapping direction based on the change of RF borders, instead of the change of RF centers used above. After the standardization of the recording configurations, the fRF and saccade target were on the right side of cRF. We chose the rightmost position of the RF contour as the landmark (the black cross in Fig. 6a). The results were shown in Fig. 6b and were generally consistent with those in Fig. 4 based on the RF centers.

Discussion

We studied LFP-defined RFs recorded from area FEF when monkeys performed a delayed saccade task. We analyzed the LFPs in four frequency bands: alpha, beta, low-gamma, and high-gamma. We found that during the initial fixation (the current period), RFs derived from these frequency bands were well correlated with the firing-rate-defined RFs obtained from the same recording sessions. The correlation is particularly strong for the alpha and high-gamma RFs. We then examined the remapping of the LFP-defined RFs during the delay and perisaccadic periods. Compared with the beta and low-gamma RFs, the alpha and high-gamma RFs showed significant remapping in greater numbers of the recording sessions. We therefore focused on the alpha and high-gamma RFs to analyze remapping characteristics in detail. We found that for the delay period, the high-gamma RFs shifted significantly towards a direction close to the initial fixation point, but the alpha RFs did not. During the perisaccadic period, the high-gamma RFs first shifted towards the target (convergent remapping) after the probe onset, then towards the fRF direction (forward remapping) around the time of saccadic onset and offset, and finally towards the target again well after the saccade. These remapping properties are similar to those of the firing-rate RFs we reported previously[4]. In contrast, the alpha RFs shifted consistently towards the fRF direction (forward remapping) over the entire perisaccadic period.

Our study and that of Chen et al.[20] found different proportions of recording sessions with well-defined RFs. For the beta, low-gamma, and high-gamma bands, the proportions in our study (beta, 32.8%; low-gamma, 16.1%; and high-gamma, 43.0%) were higher than those in Chen et al. (beta, ~10%; low-gamma, ~10%; and high-gamma, 29.74%). For the alpha band

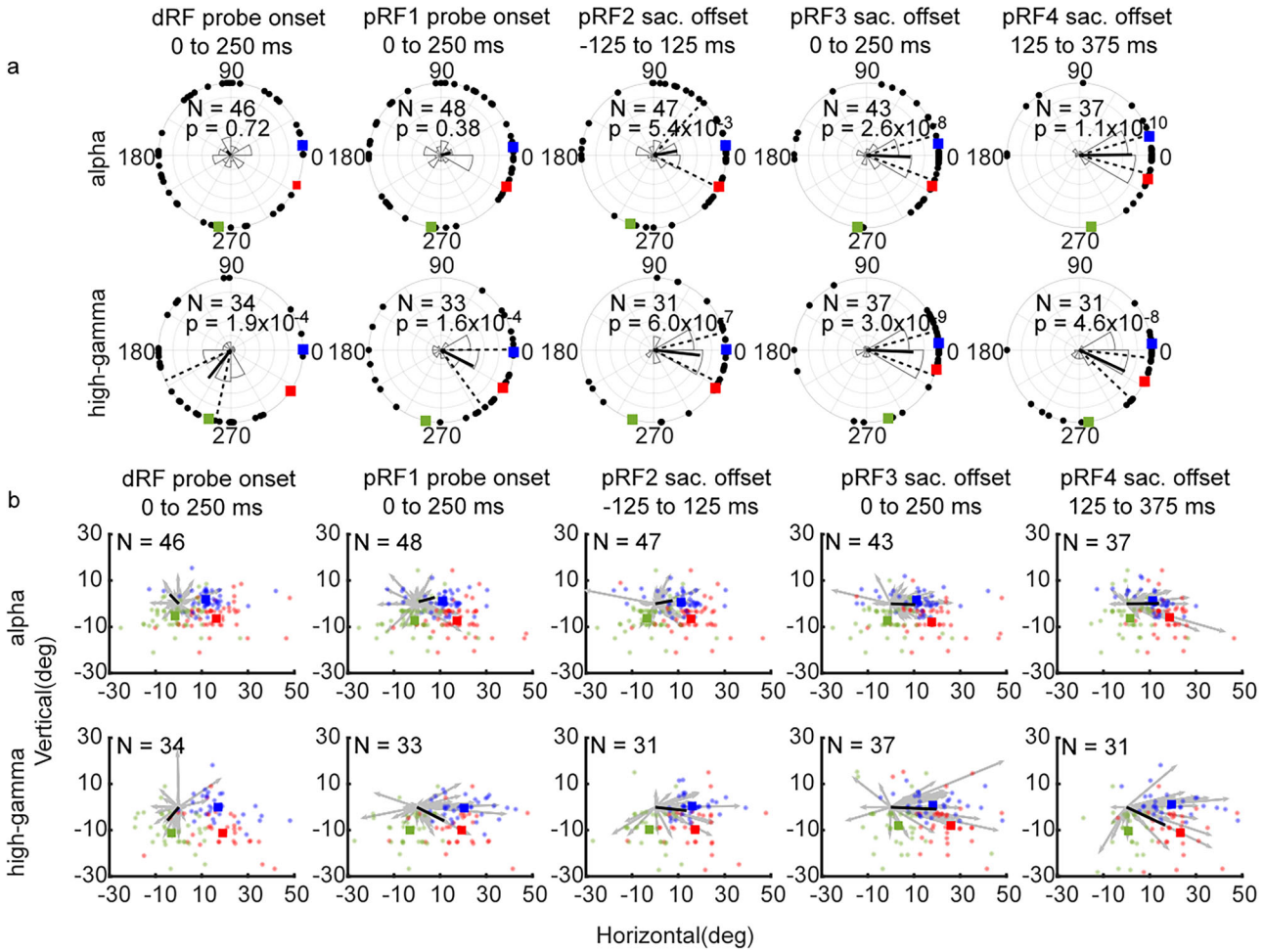

Fig. 4 | RF remapping derived from alpha and high-gamma bands. a The polar plot of RFRF remapping in derived from alpha (first row) and high-gamma (second row) bands during different periods (columns). In each polar plot, we aligned the centers of cRFs at the center of the polar plot and saccade directions along the positive horizontal. The circular mean directions of the fRFs (forward), saccade targets, and fixation points are indicated by the blue, red and green squares, respectively. Each small black dot represents the shift direction of an RF from a recording session and the thick black line represents the circular mean whose significance was indicated by the *p* values from Rayleigh test. The black dotted line indicates the 95% confidence interval of the mean direction. *N*: the number of recording sessions. **b** The vector plot of RF remapping derived from alpha (first row) and high-gamma (second row) bands. In each panel, we aligned the centers of cRFs at (0,0) and saccade directions along positive horizontal. The fRF center, the saccade target and fixation point of a recording session are shown as blue, red and green dots, respectively. Their mean positions are shown as the blue, red, and green squares, respectively. Each gray arrow represents the RF shift vector for each recording session. The black line is the vector determined by calculating the mean direction and mean amplitude of the individual vectors.

Fig. 5 | RFs from alpha and high-gamma bands show different remapping patterns. Each small black dot represents the pRF of a recording session. Its pRF-to-target distance is plotted against its pRF-to-fRF distance. The *p* values indicate that the pRFs are significantly closer to the fRFs than to the targets (Wilcoxon signed-rank test).

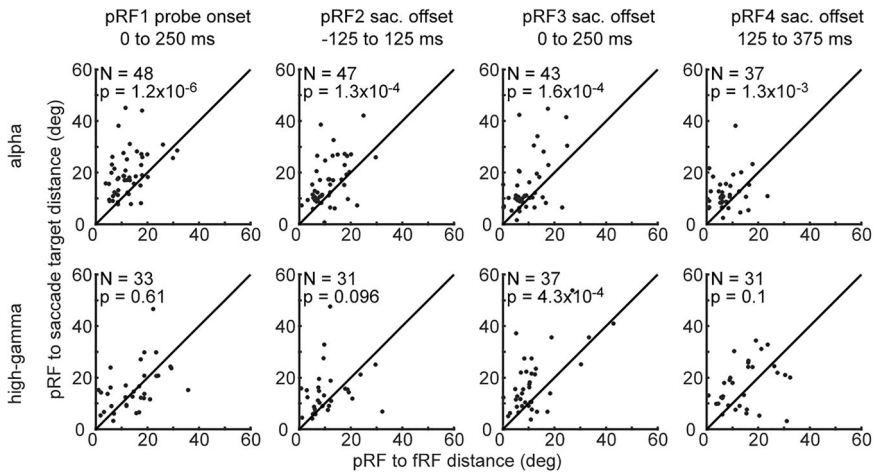

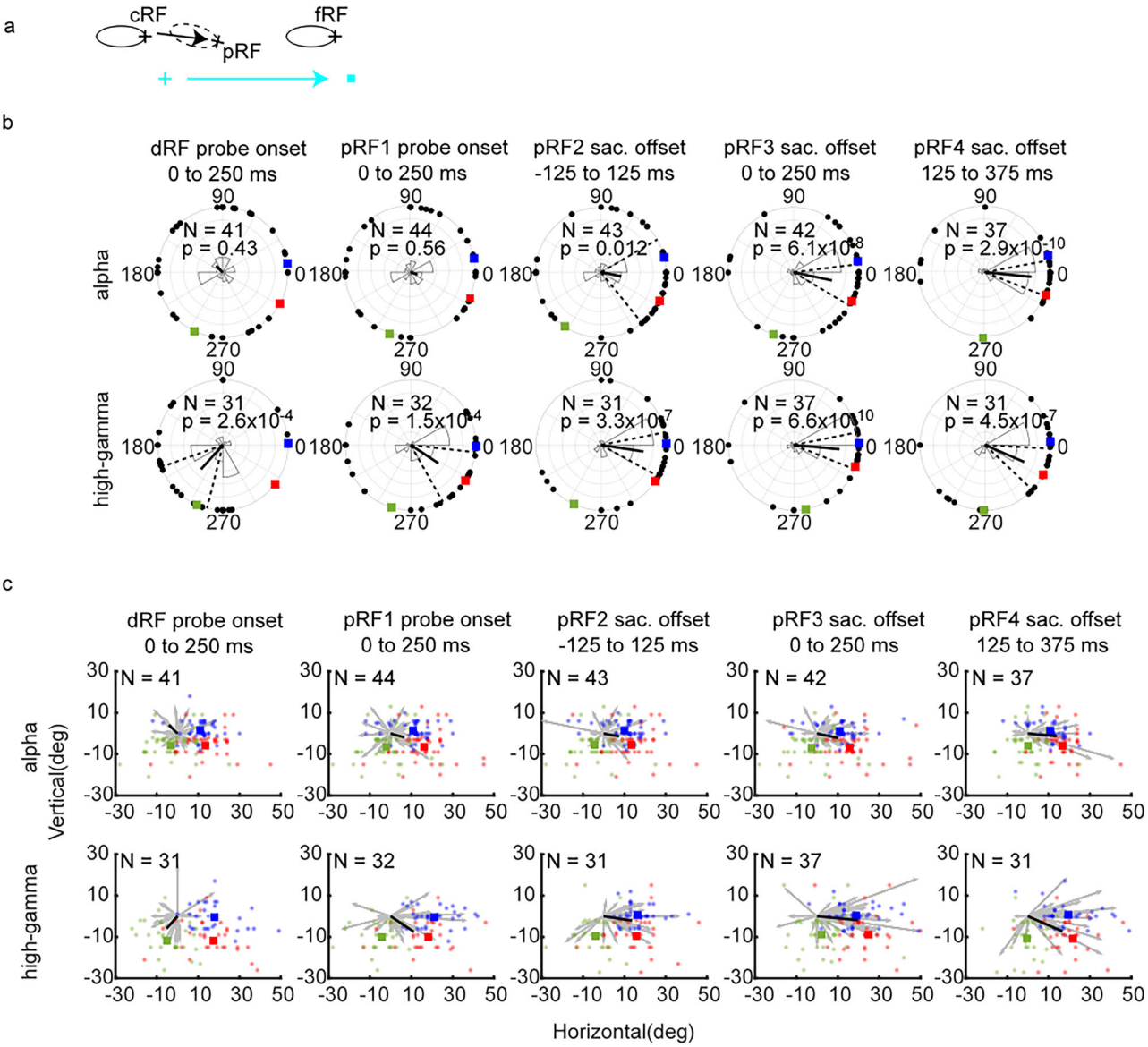

Fig. 6 | RF remapping derived from alpha and high-gamma bands calculated based on the change of the RF border. a The illustration of how to calculate RF remapping based on the change of the RF border. The rightmost position of the RF boarder is set as the landmark (black cross) to calculate the direction of RF remapping. **b** The polar plot of RF remapping direction in alpha (first row) and high-gamma (second row) bands during different periods (columns). **c** The vector plot of RF remapping derived from alpha (first row) and high-gamma (second row) bands. The figure formats are the same as that of Fig. 4.

the proportion in our study (33.0%) was lower than that in Chen et al. (52.2%). At least two factors might contribute to these differences. First, the criteria for the RF definition were different. We used a contour criterion and a completeness criterion (see "Methods") to define RFs, whereas Chen et al. defined the RFs by using mutual information (MI) between the responses and the probe locations. To assess this possibility, we also analyzed our data by using Chen et al.'s RF definition. We found higher proportions of recording sessions with RFs in all four bands (alpha, 61.63%; beta, 57.91%; low-gamma, 42.56%; high-gamma, 66.28%) than those reported by Chen et al. Second, the two studies used different recording techniques. We did single-electrode recordings, whereas Chen et al. did multi-electrode recordings. Single-electrode recording might make the online analysis easier. Indeed, during data collection, we first measured the RFs online with a fixation task (Fig. 1a) and only if there were visible RFs, did we proceed to the remapping task (Fig. 1b). This could lead to higher proportions of sessions with well-defined RFs. Whether these two factors could explain the different proportions between our study and that of Chen et al. requires further investigation.

The convergent and forward RF remapping are driven by attention and CD, respectively[1,4,6,11,16–18,27–29]. In the present study, high-gamma RFs showed dynamic changes of the remapping direction during the delay and perisaccadic periods (Figs. 4–6), covering both the convergent and the forward directions. This suggests that high-gamma RFs were modulated by both attention and the CD (at different times). In contrast, alpha RFs showed only forward shift in the perisaccadic period (Figs. 4–6), suggesting that they were primarily modulated by the CD. These findings are consistent with the previous reports that the activities of higher frequencies (≥40 Hz) are strongly modulated by attention, while those of lower frequencies are less modulated by attention[30].

As we noted in the Introduction, Zirnsak et al.[18] and Chen et al.[20] found only convergent remapping of pRFs defined by either firing rates or LFPs in FEF. In contrast, we were able to measure both convergent and forward remapping, via either firing rates[4] or LFPs (this study). This difference might be attributable to the different tasks used. In Zirnsak et al. and Chen et al.'s experiments, the target onset was also the saccade "go" signal, whereas we used a delayed saccade task to separate in time the attentional effect of the

target onset and the CD effect around the saccade. Note, however, that studies using paradigms similar to that of Zirnsak et al. (without the delay)[18,20] also found both forward and convergent remapping in V4[10,11] and MT[9]. Also note that the spatiotemporal properties of RF remapping can be remarkably different in different areas. For instance, the convergent remapping occurred around the time of saccades[18,20] or before saccades[4] in FEF whereas it occurred long after the saccade end in V4[11].

LFPs likely reflect activities of a population of neurons and neuronal processes near the recording electrode (but the spiking activities of neuron(s) closest to the electrode are filtered out). Then, our finding of significant correlations between LFP- and firing-rate-defined RFs suggests that although FEF, like other high-level areas, does not have a sharp topographic map of the visual space[31], FEF neurons with similar RFs appear to cluster together. It has also been suggested that LFPs represent synaptic inputs to the neuronal population near the recording electrode and that alpha and high-gamma bands of LFPs represent synaptic inputs from other brain areas and the local circuits, respectively[25,26]. If so, then our findings that the alpha RFs showed only forward remapping whereas the high-gamma RFs showed both forward and convergent remapping (at different times) suggest that convergent remapping might be generated locally in FEF whereas forward remapping might have both local and distant contributions. Both the local origin and the early occurrence of convergent remapping in FEF (discussed above) agree with the argument of Chen et al. that FEF might be an important brain region that generates convergent remapping[20]. Further studies are needed to determine the origins and propagations of RF remapping in the brain.

Method

Animal preparations

We used three male adult rhesus monkeys (macaque mulatta) weighted from 9 to 11 kilograms in the experiments. With a sterile surgical procedure, we implanted eye coils (Crist Instrument Sclera, sample rate at 2.7 KHz) to monitor the position of the eyes and a head post to restrain the head movements. For each monkey, we also implanted a recording chamber (2 cm diameter) centered at FEF for single-unit and LFP recording. The experimental protocol was approved by the Ethics Committee of Beijing Normal University. We have complied with all relevant ethical regulations for animal use.

Electrophysiological data acquisition

We drove single insulated tungsten microelectrodes (0.3 ~ 1.0 MΩ, FHC, USA) into the cortex with micromanipulators (NAN Instruments, Israel) and recorded the electrophysiological activities, including spikes and LFPs with AlphaLab SNR (Alpha Omega, Israel), which amplified and filtered the signal. The signal was divided into spikes (268 Hz ~ 8036 Hz) and LFPs (below 268 Hz). The sampling rate of LFPs was 1376 Hz.

Experimental setup

We ran the experiments with a QNX computer (REX; NIH, Bethesda, MD) and presented all the visual stimuli on an LED monitor (55 inch, 1920 × 1080 pixels, SAMSUNG) with a refresh rate of 60 Hz. The monkeys sat in monkey chairs 57 cm from the monitor in a dark room. The monitor covered an area of 60° × 90°at the viewing distance, but because of the frames that provided a magnetic field for measuring eye position, the actual viewing area was about 54° × 84°.

Behavioral tasks

Fixation task (Fig. 1a). We used this task to do pilot mapping of RFs of single units. Each trial started with a fixation point, which was a 0.3° × 0.3° red square, appearing at the center of the screen for 2800 ms. Monkeys were required to maintain fixation until the fixation point disappeared; otherwise, the trial was aborted. After monkeys acquired the fixation for 500 ms, six visual probes, each a 1° × 1° white square, appeared sequentially and randomly at one of the 2D array locations on the screen. The duration of each visual probe was 33 ms, and the interval between two successive probes was 400 ms. For each recording session, we first used a 5 × 8 array (with a 6° distance between adjacent locations) on the visual hemifield contralateral to the recording hemisphere, covering an area of 24° (horizontal) × 42° (vertical). If the RF exceeded the area, we increased the array to 9 × 10 (48° × 54°). We did not record units whose RFs could not be covered by the 9 × 10 array.

Delayed saccade task (Fig. 1b). After measuring the RF of a unit with the fixation task above, we proceeded to the delay saccade task for the monkeys. We tailored the array of probe positions to cover the unit's cRF-fRF region and the target region, according to the RF location and size, and the planned saccade target. The trial started with a fixation point (red square, 0.3° × 0.3°) appearing on the screen. Monkeys were trained to look at the fixation point for as long as it was on. 800 ms after achieving fixation, a saccade target (also 0.3° × 0.3° red square) appeared at another screen location. However, monkeys had to maintain fixation at the fixation point until the disappearance of fixation point 500 ms later, which was the go signal for monkeys to make a saccade to the saccade target. After the completion of the saccade, monkeys had to fixate at the saccade target until it disappeared 1000 ms later. In each trial, four white 1° × 1° visual probes were presented briefly (33 ms) at random locations of the probe array, one in each of the following periods: 400 ms after the monkeys achieved initial fixation (current or pre-target period), 100 ms after the saccade target appeared (delay period), 80 ms after the fixation point disappeared (perisaccadic period), and 700 ms after the fixation point disappeared (post-saccadic or future period). We denote a cell's RFs measured from these periods as its cRF, dRF, pRF, and fRF, respectively. Across recording sessions, the probe array varied from 4 × 5 to 10 × 12 positions, with 5 × 8, 5 × 9, and 6 × 8 the most common. The spacing between adjacent positions (along both horizontal and vertical axes) varied from 2° to 6°, with 6° the most common. The saccade amplitude varied from 5° to 30°, with 15° and 20° the most common. Despite our effort, the RFs of some recording sessions were not measured sufficiently complete because of the limited display area and large RFs and/or large saccades; these recording sessions were excluded (see Data analyses).

In the actual experiments, the initial fixation point and the target were both red squares, but for illustration, we represented them as cyan crosses and squares, respectively, in the figures.

For both tasks, we used a 6° × 6° fixation window for monkeys Mi and Vd, and a 10° to 14° window for monkey Ba. Despite the relatively large window sizes, the eye positions of all three monkeys were very stable during the time intervals in which the RFs were measured (Supplementary Fig. 1).

Data analysis

The original objective of our experiment was to study the remapping of firing-rate-defined RFs of single neurons, and this part of the data was published recently[4,5]. Since the recording electrodes picked up LFPs as well as spiking activities, we analyzed the LFPs in this study. While Wang et al. and Yang et al. [4,5,32] included single units from both LIP and FEF, our analysis focused exclusively on the LFP data from FEF because we did not have sufficient LFP data from LIP to produce robust results against variations of analysis parameters. In total, 430 FEF sessions were recorded. We used a second-order IIR notch filter to remove the 50 Hz component (the frequency of the AC power source) and its harmonics from the LFPs. The filter bandwidth was 0.1. This was done in Matlab (2020b) with functions iirnotch and filtfilt.

Power spectral density (PSD) of LFPs. We computed the PSD using Thomson's multitaper method[33], in which the taper type was Slepian and the product of time and half-bandwidth was 2 (pmtm in Matlab). We followed Chen et al.[20] to choose 250 ms windows for PSD analysis. For each trial, the baseline PSD was calculated from −250 to 0 ms before the probe onset during the current period. The stimulated PSD was estimated from 0 to 250 ms after the probe onset during the current, delay and post-saccadic periods. The stimulated PSDs during perisaccadic period were

estimated from 0 to 250 ms after perisaccadic probe onset (pRF1), and from −125 to 125 ms (pRF2), 0 to 250 ms (pRF3) and 125 to 375 ms (pRF4) relative to the saccadic offset. The average saccadic reaction time of three monkeys was 225.8 ms, and the average time difference between perisaccadic probe onset and saccadic offset was 216.1 ms. The time window of pRF1, pRF2, pRF3 and pRF4 were about 0 ms to 250 ms, 91.1 ms to 341.6 ms, 216.1 ms to 466.1 ms and 341.1 ms to 591.1 ms after the perisaccadic probe onset, respectively. We calculated the PSDs of the alpha (8–12 Hz), beta (12–30 Hz), low-gamma (30–80 Hz) and high-gamma (80–150 Hz) bands for each trial, probe location and period, then averaged PSD across trials for each probe location and period.

Criteria for RFs derived from LFPs and spiking activities. We calculated the mean stimulated PSD at each probe location during the current period (Fig. 1b), found the location with the maximum PSD, and then compared it with the mean baseline PSD of the same probe location. If the stimulated PSD was greater than the baseline PSD by 1 SD of the baseline PSD, we defined the LFP as having significant visual responses. Otherwise, the LFP data were excluded for further analysis. Next, we normalized the PSDs across probe locations according to:

$$r'_{xy} = \frac{r_{xy} - r_{\min}}{r_{\max} - r_{\min}}$$

where r_{xy} and r'_{xy} were the PSDs at the array location (x, y) before and after the normalization, respectively, and $r_{\max}$ and $r_{\min}$ were the maximum and minimum PSDs across probe locations, respectively. We linearly interpolated the normalized PSDs across all probe locations. To determine RF center location, we first found the locations where the normalized PSDs exceeded 90% of the maximum normalized PSD (contour criterion), and set the PSDs at the rest of the probe locations to 0. We then applied the Matlab 'bwconncomp' function to find how many separate patches were in the RF. If there were only one patch, we chose it. If there were more than one patch, we chose the largest patch if its size was more than twice of the next largest patch. Otherwise, the LFP data were excluded for further analysis. Additionally, we required that 80% of the patch contour was within the sampled probe array (completeness criterion) and the minimum number of trials at each probe location within the patch was 5. For most of the RFs (with remapping) we measured, their contours were completely within the sampled array of locations (Supplementary Table 1). For the RFs whose contours were not fully covered by sampled array of probe positions, we first used the edges of the sampled array to complete the contour and then required that the measured contour was no less than 80% of the total contour. Finally, we calculated the center of mass of the chosen patch as the RF center $(\bar{x}, \bar{y})$:

$$\bar{x} = \frac{1}{s}\sum_x \sum_y r'_{xy} x$$

$$\bar{y} = \frac{1}{s}\sum_x \sum_y r'_{xy} y$$

$$S = \sum_x \sum_y r'_{xy}$$

where x and y denoted the probe location.

For the firing-rate-defined RFs, we calculated the firing rates instead of PSDs using the same parameters and criteria.

Statistics and reproducibility

Criteria for remapping of LFP-defined RFs. For each recording session, to determine whether the LFP-defined RFs remapped during the delay and perisaccadic periods, we compared the centers of dRF and pRF with the center of cRF. We defined the remapping as the shift of the dRF or pRF center relative to the cRF center. To determine whether a shift was significant, we used the following bootstrap procedure: for each RF, we randomly sampled PSDs with replacement from the original datasets with the numbers of trials equal to the actual number of trials at each location, and then determined the RF center location. We repeated the process 1000 times. To determine, for example, whether the 1000 dRF centers shifted significantly from the 1000 cRF centers in the simulation, we calculated their overlaps along the axis linking the mean dRF center and cRF center, and required the overlap to be less than 10% (overlap criterion).

We used polar plots to present population results from all the recording sessions. In each polar plot, we aligned each session's cRF at the center and the saccade direction along the positive horizontal. After this procedure, if the initial fixation and saccade target were above the horizontal axis, we flipped them with respect to the horizontal axis.

We determined RFs and their remapping from the alpha, beta, low-gamma, and high-gamma bands of the LFPs. If the significance of a remapping, for example, in any one band led to the inclusion of its counterparts in all the other bands for analysis, there would be an accumulation of Type I error which would require correction. To avoid this problem, we included a remapping for analysis in a given band only when it is significant in that band regardless of tests in the other bands.

Spatial correlation between LFP- and firing-rate-defined RFs from the same recording session. To compare the RFs defined by the firing rates (RF_i) and LFPs (RF_j) during the current period, we calculate the spatial correlation between them:

$$r = \frac{\sum_x \sum_y (RF_{i,x,y} - \overline{RF_i})(RF_{j,x,y} - \overline{RF_j})}{\sqrt{(\sum_x \sum_y (RF_{i,x,y} - \overline{RF_i})^2)(\sum_x \sum_y (RF_{j,x,y} - \overline{RF_j})^2)}}$$

where $RF_{i,x,y}$ and $RF_{j,x,y}$ denote the activities of RF_i and RF_j at probe location (x, y); $\overline{RF_i}$ and $\overline{RF_j}$ denote the mean activities of RF_i and RF_i across all probe locations, respectively. For each pair of signals, we assess the significance of the correlation through a nonparametric permutation test with 1000 repetitions.

Reporting summary

Further information on research design is available in the Nature Portfolio Reporting Summary linked to this article.

Data availability

The data used in this paper are publicly available in Figshare with the identifier https://doi.org/10.6084/m9.figshare.29133431.v1 (ref. 34).

Received: 17 November 2024; Accepted: 30 May 2025;
Published online: 12 June 2025

References

1. Sommer, M. A. & Wurtz, R. H. Influence of the thalamus on spatial visual processing in frontal cortex. *Nature* **444**, 374–377 (2006).
2. Umeno, M. M. & Goldberg, M. E. Spatial processing in the monkey frontal eye field. I. Predictive visual responses. *J. Neurophysiol.* **78**, 1373–1383 (1997).
3. Umeno, M. M. & Goldberg, M. E. Spatial processing in the monkey frontal eye field. II. Memory responses. *J. Neurophysiol.* **86**, 2344–2352 (2001).
4. Wang, X. et al. Perisaccadic and attentional remapping of receptive fields in lateral intraparietal area and frontal eye fields. *Cell Rep.* **43**, 113820 (2024).
5. Wang, X. et al. A circuit model for transsaccadic space updating and mislocalization. *Proc. Natl. Acad. Sci. USA*. **122**, e2422911122 (2025).
6. Duhamel, J.-R., Colby, C. L. & Goldberg, M. E. The updating of the representation of visual Space in parietal cortex by intended eye movements. *Science* **255**, 90–92 (1992).

7. Wang, X. et al. Perisaccadic receptive field expansion in the lateral intraparietal area. *Neuron* **90**, 400–409 (2016).
8. Akbarian, A., Clark, K., Noudoost, B. & Nategh, N. A sensory memory to preserve visual representations across eye movements. *Nat. Commun.* **12**, 6449 (2021).
9. Niknam, K. et al. Characterizing and dissociating multiple time-varying modulatory computations influencing neuronal activity. *PLoS Comput. Biol.* **15**, e1007275 (2019).
10. Hartmann, T. S., Zirnsak, M., Marquis, M., Hamker, F. H. & Moore, T. Two types of receptive field dynamics in area V4 at the time of eye movements? *Front. Syst. Neurosci*. **11**, 13 (2017).
11. Neupane, S., Guitton, D. & Pack, C. C. Dissociation of forward and convergent remapping in primate visual cortex. *Curr. Biol.* **26**, R491–R492 (2016).
12. Nakamura, K. & Colby, C. L. Updating of the visual representation in monkey striate and extrastriate cortex during saccades. *Proc. Natl. Acad. Sci. USA* **99**, 4026–4031 (2002).
13. Denagamage, S., Morton, M. P., Hudson, N. V. & Nandy, A. S. Widespread receptive field remapping in early primate visual cortex. *Cell Rep.* **43**, 114557 (2024).
14. Churan, J., Guitton, D. & Pack, C. C. Perisaccadic remapping and rescaling of visual responses in macaque superior colliculus. *PLoS ONE* **7**, e52195 (2012).
15. Walker, M. F., Fitzgibbon, E. J. & Goldberg, M. E. Neurons in the monkey superior colliculus predict the visual result of impending saccadic eye movements. *J. Neurophysiol.* **73**, 1988–2003 (1995).
16. Connor, C. E., Preddie, D. C., Gallant, J. L. & Van Essen, D. C. Spatial attention effects in macaque area V4. *J. Neurosci.* **17**, 3201–3214 (1997).
17. Tolias, A. S. et al. Eye movements modulate visual receptive fields of V4 neurons. *Neuron* **29**, 757–767 (2001).
18. Zirnsak, M., Steinmetz, N. A., Noudoost, B., Xu, K. Z. & Moore, T. Visual space is compressed in prefrontal cortex before eye movements. *Nature* **507**, 504–507 (2014).
19. Marino, A. C. & Mazer, J. A. Perisaccadic updating of visual representations and attentional states: linking behavior and neurophysiology. *Front. Syst. Neurosci*. **10**, 3 (2016).
20. Chen, X., Zirnsak, M. & Moore, T. Dissonant representations of visual space in prefrontal cortex during eye movements. *Cell Rep.* **22**, 2039–2052 (2018).
21. Neupane, S., Guitton, D. & Pack, C. C. Coherent alpha oscillations link current and future receptive fields during saccades. *Proc. Natl. Acad. Sci. USA* **114**, E5979–E5985 (2017).
22. Berens, P. Comparing the feature selectivity of the gamma-band of the local field potential and the underlying spiking activity in primate visual cortex. *Front. Syst. Neurosci*. **2**, 2 (2008).
23. Kreiman, G. et al. Object selectivity of local field potentials and spikes in the macaque inferior temporal cortex. *Neuron* **49**, 433–445 (2006).
24. Kruse, W. & Eckhorn, R. Inhibition of sustained gamma oscillations (35–80 Hz) by fast transient responses in cat visual cortex. *Proc. Natl. Acad. Sci. USA* **93**, 6112–6117 (1996).
25. Belitski, A. et al. Low-frequency local field potentials and spikes in primary visual cortex convey independent visual information. *J. Neurosci.* **28**, 5696–5709 (2008).
26. Ray, S. & Maunsell, J. H. R. Differences in gamma frequencies across visual cortex restrict their possible use in computation. *Neuron* **67**, 885–896 (2010).
27. Golomb, J. D. & Mazer, J. A. Visual remapping. *Annu. Rev. Vis. Sci.* **7**, 257–277 (2021).
28. Wurtz, R. H. Neuronal mechanisms of visual stability. *Vis. Res.* **48**, 2070–2089 (2008).
29. Sommer, M. A. & Wurtz, R. H. Brain circuits for the internal monitoring of movements. *Annu. Rev. Neurosci.* **31**, 317–338 (2008).
30. Prakash, S. S., Das, A., Kanth, S. T., Mayo, J. P. & Ray, S. Decoding of attentional state using high-frequency local field potential is as accurate as using spikes. *Cereb. Cortex* **31**, 4314–4328 (2021).
31. Schall, J., Morel, A., King, D. & Bullier, J. Topography of visual cortex connections with frontal eye field in macaque: convergence and segregation of processing streams. *J. Neurosci.* **15**, 4464–4487 (1995).
32. Yang, L., Jin, M., Zhang, C., Qian, N. & Zhang, M. Distributions of visual receptive fields from retinotopic to craniotopic coordinates in the lateral intraparietal area and frontal eye fields of the macaque. *Neurosci. Bull.* **40**, 171–181 (2024).
33. Thomson, D. J. Spectrum estimation and harmonic analysis. *Proc. IEEE* **70**, 1055–1096 (1982).
34. JIN MIN. LFP-defined RF remapping. https://doi.org/10.6084/m9.figshare.29133431.v1 (2025).

Acknowledgements

This work was supported by the National Natural Science Foundation of China (32030045, 82071454) and STI2030-Major Projects +2021ZD0204300, and by the U.S. National Eye Institute (R01 EY032938).

Author contributions

M.Z., M.J. and L.Y. designed this work; M.J., L.Y. and F.J. collected the data; M.J. and L.Y. analyzed the data; M.Z., N.Q. and M.J. wrote the manuscript. M.J., L.Y. and F.J. are the co-first authors.

Competing interests

The authors declare no competing interests.

Additional information

Supplementary information The online version contains supplementary material available at https://doi.org/10.1038/s42003-025-08324-0.

Correspondence and requests for materials should be addressed to Mingsha Zhang.

Peer review information *Communications Biology* thanks Sujaya Neupane and the other, anonymous, reviewers for their contribution to the peer review of this work. Primary Handling Editor: Jasmine Pan. A peer review file is available.